What Causes Tides?

Yongfeng Yang

Bureau of Water Resources of Shandong Province

Abstract Tide (the daily cycle of high and low water) has been known for thousands of years. The widely accepted theory for this movement is the attractive mechanism, that's to say, the Moon's gravitational attraction yields a pair of water bulges on the Earth, an Earthly site will periodically pass these bugles and thus undergo alternation of high and low water as the Earth spins. However, an in-depth investigation of global tide-gauge data shows these bulges of water nonexistent. This absence suggests that tide cannot be explained by the attractive mechanism. Here we propose, the Earth's rotations about the centre of mass of the Earth-Moon system and around the Sun create some centrifugal effects to stretch the Earth's body; the deformed solid Earth generates oscillation for ocean basin as the Earth rotates, forming water movement between all the parts of the basin and further the rise and fall of water level around the globe. A modelling test shows that the *RMS* (Root Mean Square) deviation of amplitude calculated against observation for deep ocean (34 sites) and shelf-coastal regions (42 sites) are approximately 6.16 and 10.59 cm.

Keywords tide, wave, the Earth-Moon system, the centrifugal effect, deformation of solid Earth, oscillating vessel, ocean basin, tide prediction

1 Introduction

1.1 A brief retrospect of tidal theories

From antiquity it has been known that coastal seas always perform daily regular water movements of rise and fall. Since these movements are closely related to the frequently coastal activities, explaining them has undoubtedly tested human wisdom. Aristotle (384-322 BC) was highly perplexed by the phenomenon and vaguely attributed it to the

rocky nature of the coastline. The early Chinese considered tides as the beating of the Earth's pulse and alternately, it was believed to be caused by the Earth's breathing. Others thought tides were caused by the different depths of ocean water. Galileo theorized that the rotations of the Earth around the Sun and about its axis induced motion within the sea to generate the tides. The majority certainly linked tidal action to the influence of the Moon and of the Sun. Seleucus (2nd century BC) was the first to consider this connection and concluded the height of tide was correlated with the Moon's position relative to the Sun. However, the exact determination of how the Moon and Sun caused tides was unknown. A few Arabic explanations proposed that the Moon used its rays to heat and expand the water. Descartes argued that space was full of ethereal substance and the resulting stresses between the ether and the Earth's surface gave birth to tides when the Moon orbited the Earth. In contrast, Kepler and Newton defined the action as the attraction of the Moon and Sun on water. Newton concluded the Moon's gravitation caused a pair of water bulges on the Earth. In consideration of the complexity of actual oceans and currents, Laplace developed a set of hydrodynamic equations. Together with the following endeavours (made by William Thomson, Baron Kelvin, Henri Poincaré, Arthur Thomas Doodson, etc.,), the idea of the gravitational attractions of the Moon and Sun on water, i.e., the attractive mechanism, was increasingly consolidated and became the cornerstone of modern tidal theories. A fuller review of tidal theory may be seen in these works (Pugh 1987; Cartwright 1999; Deacon 1971; Pugh and Woodworth 2014). Undoubtedly, the physics of tides involves in a variety of fields ranging from the orbit of celestial objects (the Moon and the Sun, for instance), the mixing of the oceans, solid-Earth geophysics and coastal flooding (Lambeck 1988; Munk 1997; Vlasenko et al. 2005). In the past decades a rapid growth of ocean tide models greatly facilitated spatial and ground measurements (Pekeris et al. 1969; Schwiderski 1979; Fu and Cazenave 2001; Visser et al. 2010), tidal dynamics and energy dissipation were also studied (Stammer et al. 2014), the investigation on internal tides becomes considerably active (Gargett and Hghes 1972; Phillips 1974; Shepard 1975; Garrett and Munk 1979; Gao et al. 2013; Shanmugam 2014), all these help us realize a better understanding of tide.

1.2 An examination of the attractive mechanism

The attractive mechanism postulates the Earth orbits about the centre of mass of the Earth-Moon system, this makes all particles of the Earth travel around in the circles of same radius. The force responsible for these circular or curved motions is treated as centripetal force. The centripetal force necessary to maintain each particle in this rotation is the same as for the particles at the centre. For particles nearer the Moon, its gravitational attraction on them is greater than the centripetal force. Further away, the Moon's gravitational attraction is weaker than the centripetal force. The difference between the centripetal force and the Moon's gravitational attraction is the tide-generating force (Pugh 1987; Pugh and Woodworth 2014). The tide-generating force is further decomposed into two components of respectively vertical and horizontal to the Earth's surface. The vertical can be compensated by Earth's gravity, but the horizontal cannot be counteracted in the same manner and causes particles to move in the direction of the force. The net result of the tidal forces acting on a watery Earth is to move water towards positions nearest to and farthest from the Moon. This eventually yields two bulges of water along the Earth-Moon line and a depression of water in a ring around the Earth halfway between the two bulges (Pugh 1987; Robert 2008; Pugh and Woodworth 2014). For an Earthly site it would pass through the two bulges of water and the depression as the Earth spins and hence undergoes two cycles of high and low water per day. Similarly, another two bulges of water along the Earth-Sun line and another depression of water between these two bulges are also yielded due to the Sun's gravitational attraction on water. When these two types of bulges and depressions are combined together, they reinforce or cancel each other to generate the two cycles of high and low water per month (Pugh 1987; Robert 2008; Pugh and Woodworth 2014).

More than 300 years, most of people had been led by these bulges of water to know tide, and the paradigm of the two bulges of water has been extensively included in many textbooks. However, the existence of these bulges of water has never been strictly investigated. Nowadays, many large tide data collections like UHSLC (University of Hawaii Sea Level Center), PSMSL (Permanent Service for Mean Sea

Level), and BODC (British Oceanographic Data Center) provide condition for us to do this work. If there were two bulges of water on the Earth, there would be a thing to happen, i.e., an Earthly site that enters into these bulges of water would undergo high water as the Earth spins around its axis (Fig. 1(A)). From a viewpoint of spherical geometry, if water responds to the Moon's gravitational attraction at a timely manner, i.e., forming two bulges of water on the Earth, these bulges should be directed along the Earth-Moon line, we believe that an Earthly site, when its lunar angle θ, which is the angle of this site (marked with *S*, for instance) and the Moon with respect to the Earth's centre, falls into a phase of 0^o~45^o and 135^o~180^o, must have entered into the two bulges of water and trend to perform high water, whereas when its lunar angle falls into a phase of 45^o~135^o, it must have got out of the two bulges and trend to perform low water. However, even if the response of water to the Moon's gravitational attraction is not at a timely manner, i.e., the two bulges are not directed along the Earth-Moon line, an Earthly site still would enter into or get out of these bulges of water as the Earth spins, and thus trends to perform high or low water. Specifically, the frame of the two bulges of water requires a concentration of high or low waters for all sites as the Earth spins. We employ hourly tide-gauge data of 229 globally-distributed sites from GLOSS database-UHSLC to examine this expectation. This dataset presently provides free access for anyone to obtain the monthly, daily, or hourly tide-gauge data through a DODS server. The geographic positions (latitude and longitude, for instance) of these sites are listed in Table 1. Both the position of a site and the Moon's position allow to exactly know the lunar angle. Tide-gauge data are treated as follows: water level change of a tide gauge site is the difference of the mean of all hourly water levels of this site during the month and its hourly water level. This treatment yields a reference frame (i.e., water level is zero) for all these sites to be compared together. Difference from that expectation above, the distributions of high and low waters of all these 229 tide gauge sites, as shown in Figure 1(B), are rather scattered, no evidence to show a concentration of high or low waters at any special phase. Figure 1(B) exhibits a state of 12 independent moments (0h, 2h, 4h, …, for instance) in the day of August 13, 2014 when the Moon is about equator. We extend

this day to the whole August to examine the existence of the two bugles of water. The Moon moves around north and south of equator, if the Moon's gravitational attraction yields two bulges of water, these bulges of water would company the Moon together to transfer back and forth. In the process of this transition, the two bulges of water would require the two successive high waters of an Earthly site (if not at equator) to reversely develop, namely, for a site which is located at higher latitude, the size of one high water that this site experiences is increased/decreased whereas the size of another adjacent high water is decreased/increased. Different from this expectation, the sizes of the two successive high waters of the observed tides, as shown in Figure 1(C), are alternatively increased or decreased. In particular, the two bulges of water would require these sites located at lower latitudes to experience two high waters and two low waters during a day (i.e., the semidiurnal tides) whereas those sites located at higher latitudes to experience one high water and one low water during a day (i.e., the diurnal tides). Different from this expectation, as shown in Figure 1(D), the semidiurnal tides are extensively distributed around the globe, while the diurnal tides are less distributed, only a few places (the Karumba, Mexico gulf, Sea of Okhotsk, for instance) hold them.

Finally, no evidence is shown to support the existence of these bulges of water. Some people ascribes this absence of these bulges of water to be the influences of continents, seafloor topography, and so on, while others speculates the Moon's gravitational attraction could be unworkable in yielding these bulges of water. Despite of these arguments, we prefer to seek for the effect of this absence, namely, without these bulges of water on the Earth' surface, it is impossible for an Earthly site to get in or out of them, and also impossible for the two types of bugle (i.e., lunar and solar) to reinforce or cancel each other, consequently, the daily and fortnightly cycles of high and low water become unresolved in the attractive mechanism. This unknowing suggests some alternative explanation for tide.

Table 1 Coordinates of 229 tide gauge sites from GLOSS database-UHSLC

ID	Tide-gauge station	Latitude	Longitude	ID	Tide-gauge station	Latitude	Longitude
1	POHNPEI	6.98	158.20	286	PUERTO	-47.75	294.08
2	BETIO	1.37	172.93	288	REYKJAVIK	64.15	338.07
3	BALTRA	0.43	269.72	289	GIBRALTAR	36.12	354.65
5	MAJURO	7.10	171.37	290	PORT	-51.75	302.07
7	MALAKAL	7.33	134.47	291	ASCENSION	-7.92	345.58
8	YAP	9.52	138.13	299	QAQORTOQ	60.72	313.97
9	HONIARA	-9.43	159.95	302	BALBOA	8.97	280.43
11	CHRISTMAS	1.98	202.53	328	KO	11.80	99.82
14	FRENCH	23.87	193.72	329	QUARRY	22.30	114.22
15	PAPEETE	-17.53	210.43	331	BRISBANE	-27.37	153.17
16	RIKITEA	-23.13	225.05	332	BUNDABERG	-24.83	152.35
18	SUVA	-18.13	178.43	333	FORT	-33.85	151.23
19	NOUMEA	-22.30	166.43	334	TOWNSVILLE	-19.25	146.83
21	JUAN	-33.62	281.17	335	SPRING	-42.55	147.93
22	EASTER	-27.15	250.55	336	BOOBY	-10.60	141.92
23	RAROTONGA	-21.20	200.22	340	KAOHSIUNG	22.62	120.28
24	PENRHYN	-8.98	201.95	341	KEELUNNG	25.15	121.75
25	FUNAFUTI	-8.53	179.22	345	NAKANO	29.83	129.85
29	KAPINGAMARANGI	1.10	154.78	347	ABASHIRI	44.02	144.28
30	SANTA	0.75	269.68	348	HAMADA	34.90	132.07
31	NUKU	-8.93	219.92	349	TOYAMA	36.77	137.22
34	CABO	22.88	250.08	350	KUSHIRO	42.97	144.38
38	NUKU'ALOFA	-21.13	184.83	351	OFUNATO	39.07	141.72
39	KODIAK	57.73	207.48	352	MERA	34.92	139.83
40	ADAK	51.87	183.37	353	KUSHIMOTO	33.47	135.78
41	DUTCH	53.90	193.50	354	ABURATSU	31.57	131.42
43	PALMYRA	5.87	197.90	355	NAHA	26.22	127.67
46	PORT	-17.77	168.30	356	MAISAKA	34.68	137.62
47	CHICHIJIMA	27.10	142.18	359	NAZE	28.38	129.50
49	MINAMITORISHIMA	24.30	153.97	360	WAKKANAI	45.40	141.68
50	MIDWAY	28.22	182.63	362	NAGASAKI	32.73	129.87
51	WAKE	19.28	166.62	363	NISHINOOMOTE	30.73	131.00
52	JOHNSTON	16.75	190.48	364	HAKODATE	41.78	140.73

53	GUAM	13.43	144.65	365	ISHIGAKI	24.33	124.15
55	KWAJALEIN	8.73	167.73	370	MANILA	14.58	120.97
56	PAGO	-14.28	189.32	371	LEGASPI	13.15	123.75
57	HONOLULU	21.30	202.13	372	DAVAO	7.08	125.63
58	NAWILIWILI	21.97	200.65	381	QUINHON	13.77	109.25
59	KAHULUI	20.90	203.53	382	SUBIC	14.82	120.28
60	HILO	19.73	204.93	383	VUNG	10.33	107.07
61	MOKUOLOE	21.43	202.20	402	LAUTOKA	-17.60	177.43
71	WELLINGTON	-41.28	174.78	417	SADENG	-8.50	110.78
72	BLUFF	-46.60	168.33	418	WAIKELO	-9.40	119.23
79	CHATHAM	-43.95	183.43	419	LAMBAR	-8.73	116.07
80	ANTOFAGASTA	-23.65	289.60	420	MAUMLAKI	-7.98	131.28
81	VALPARAISO	-33.03	288.37	540	PRINCE	54.32	229.67
82	ACAJUTLA	13.58	270.17	542	TOFINO	49.15	234.08
83	ARICA	-18.47	289.67	547	BARBERS	21.32	201.88
88	CALDERA	-27.07	289.17	548	KAUMALAPAU	20.78	203.00
91	LA	-2.20	279.08	551	SAN	37.80	237.53
93	CALLAO	-12.05	282.85	552	KAWAIHAE	20.03	204.17
94	MATARANI	-17.00	287.88	554	LA	32.87	242.73
101	MOMBASA	-4.07	39.65	556	CRESCENT	41.75	235.82
103	PORT	-20.15	57.50	558	NEAH	48.37	235.38
104	DIEGO	-7.28	72.40	559	SITKA	57.05	224.65
105	RODRIGUES	-19.67	63.42	560	SEWARD	60.12	210.57
108	HULHULE	4.18	73.53	569	SAN	32.72	242.83
109	GAN	0.68	73.15	570	YAKUTAT	59.55	220.27
110	MUSCAT	23.63	58.57	571	KETCHIKAN	55.33	228.37
113	MASIRAH	20.68	58.87	574	SAND	55.33	199.50
115	COLOMBO	6.97	79.87	579	PRUDHOE	70.40	211.47
117	HANIMAADHOO	6.77	73.17	592	SOUTH	44.63	235.95
119	DJIBOUTI	11.60	43.15	595	NOME,NORTON	64.50	194.57
121	POINT	-4.67	55.53	600	USHUAIA	-54.80	291.70
122	SIBOLGA	1.75	98.77	654	CURRIMAO	18.02	120.48
123	SABANG	5.83	95.33	655	LUBANG	13.82	120.20
124	CHITTAGONG	22.23	91.83	684	PUERTO	41.48	287.03
125	PRIGI	-8.28	111.73	699	TANJONG	1.27	103.85

126	JASK	25.63	57.77	700	FARADAY	-65.25	295.73
128	THEVENARD	-32.15	133.63	701	PORT	-29.28	16.85
129	PORTLAND	-38.35	141.60	702	LUDERITZ	-26.63	15.17
142	LANGKAWI	6.43	99.75	703	SALDAHNA	-33.02	17.95
147	KARACHI	24.80	66.97	704	CAPE	-34.18	18.43
148	KO	7.83	98.43	708	SALVADOR	-12.97	321.48
149	LAMU	-2.27	40.90	729	MAR	-38.03	302.47
153	MINICOY	8.12	73.05	731	PUERTO	-42.77	294.97
155	DZAOUDZI	-12.78	45.25	737	SAN	12.58	278.30
162	CILACAP	-7.75	109.02	738	SANTA	11.23	285.77
163	BENOA	-8.75	115.22	739	EL	9.57	281.05
164	REUNION	-20.92	55.30	752	FORT	32.03	279.10
168	DARWIN	-12.47	130.85	755	VIRGINIA	25.73	279.83
171	COCOS	-12.12	96.90	762	PENSACOLA	30.40	272.78
172	ADEN	11.22	44.98	775	GALVESTON(PIER21)29	29.32	265.20
174	COCHIN	9.97	76.27	776	PUNTA	18.50	291.62
175	FREMANTLE	-32.05	115.73	777	PUERTO	19.80	289.30
176	ESPERANCE	-33.87	121.90	786	ROSEAU	15.30	298.60
181	DURBAN	-29.88	31.00	789	PRICKLEY	12.00	298.23
184	PORT	-33.97	25.63	799	PORT	18.57	287.65
185	MOSSEL	-34.07	22.33	800	ANDENES	69.32	16.15
186	KNYSNA	-34.08	23.05	801	HONNINGSVARG	70.98	25.98
187	EAST	-33.00	27.92	802	MLLOY	61.93	5.12
188	RICHARD'S	-28.78	32.10	803	RORVIK	64.87	11.25
207	CEUTA	35.90	354.68	804	TREGDE	58.00	7.57
209	CASCAIS	38.70	350.58	805	VARDO	70.33	31.10
211	PONTA	37.73	334.32	806	NOUAKCHOTT	18.10	344.05
220	WALVIS	-22.95	14.50	807	ALEXANDRIA	31.22	29.92
221	SIMON'S	-34.18	18.43	808	THULE	76.00	292.00
223	DAKAR	14.67	342.57	809	SCORESBYSUND	70.48	338.02
235	PALMEIRA	16.75	337.02	818	SMOGEN	58.35	11.22
242	KEY	24.55	278.18	819	GOTHENBURG	57.68	11.80
245	SAN	18.47	293.88	820	NUUK	64.17	308.28
253	NEWPORT	41.50	288.67	824	MARSEILLE	43.30	5.35
257	SETTLEMENT	26.72	281.00	825	CUXHAVEN	53.87	8.72

259	BERMUDA	32.37	295.30	829	TRIESTE(SARTORIO)45	45.65	13.77
260	DUCK	36.18	284.27	830	LA	43.37	351.60
261	CHARLESTON	32.78	280.07	833	NAIN	56.55	298.30
264	ATLANTIC	39.35	285.58	834	MALIN	55.37	352.67
266	CRISTOBAL	9.35	280.10	835	CASTLETOWNSEND	55.37	352.67
268	LIMON	10.00	276.97	878	BULLEN	12.18	290.98
271	FORT	14.60	298.93	906	MOULMEIN	16.48	97.62
273	BASQUES	47.57	300.87	907	SITTWE	11.68	92.77
274	CHURCHILL	58.78	265.80	908	PORT	11.68	92.77
275	HALIFAX	44.67	296.42	914	MEULABOH	5.13	96.13
283	FORTALEZA	-3.72	321.53	922	MITWARA	-10.28	40.18
276	ST-JOHN'S	47.57	307.28				

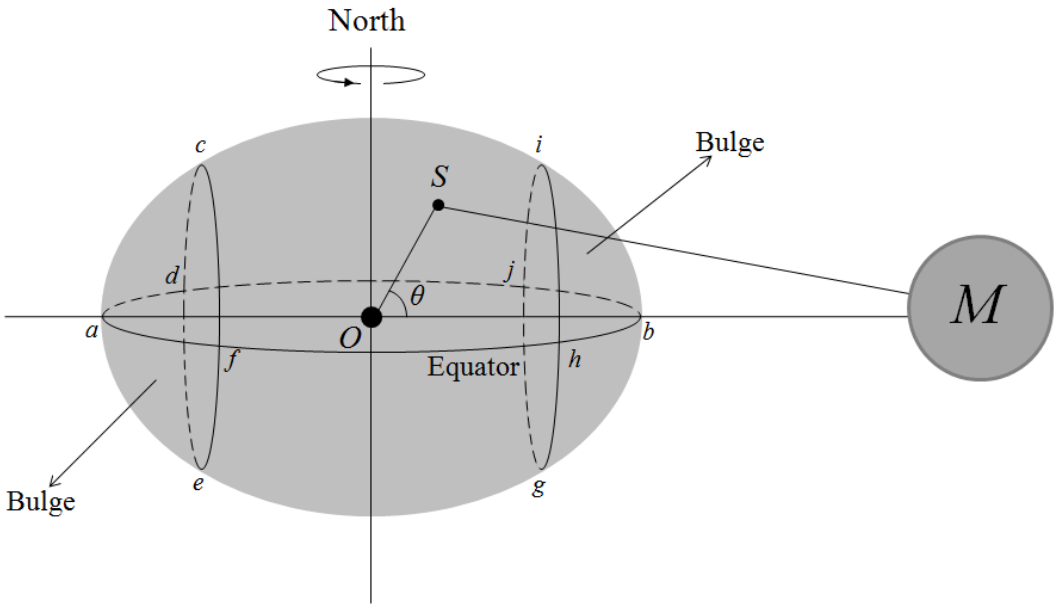

A

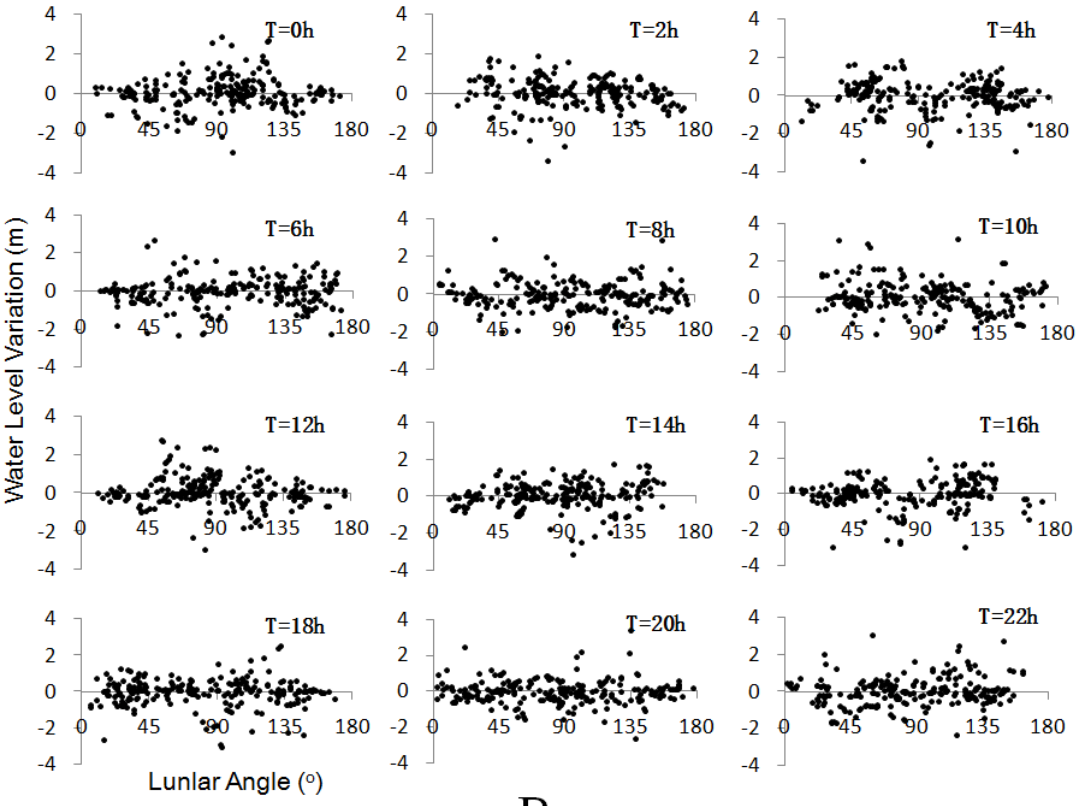
T=0h
T=2h
T=4h
T=6h
T=8h
T=10h
T=12h
T=14h
T=16h
T=18h
T=20h
T=22h
Water Level Variation (m)
Lunlar Angle (°)

B

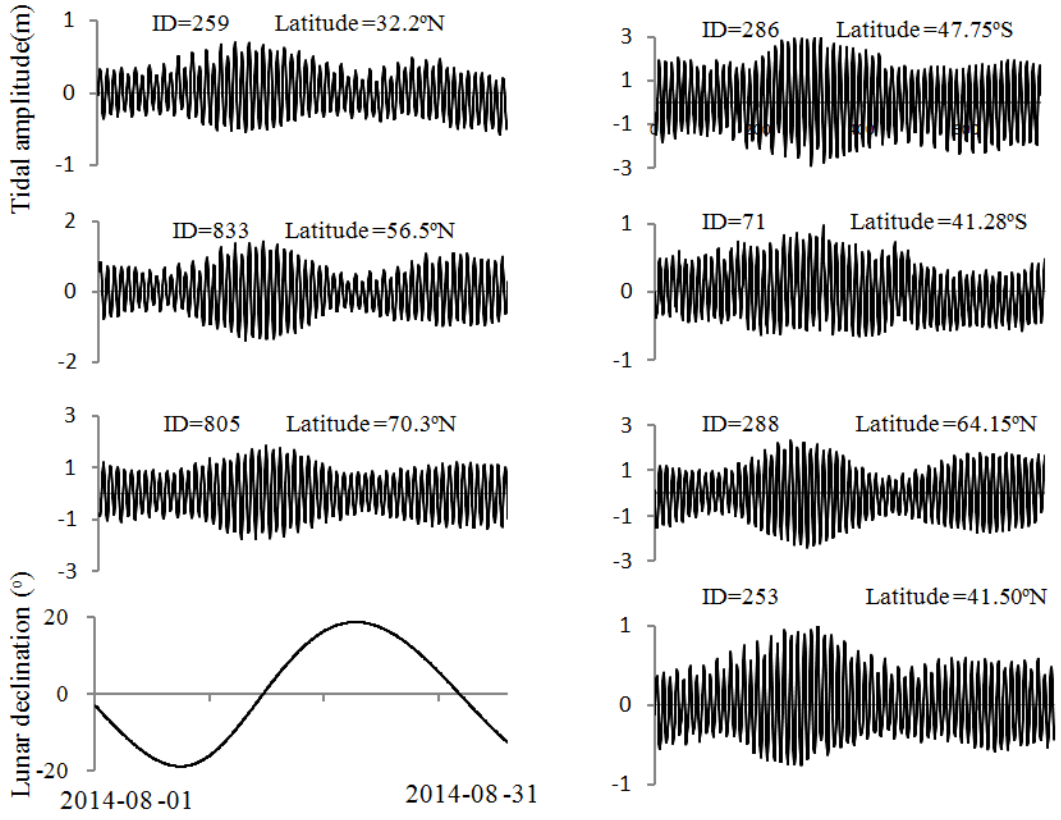
Tidal amplitude(m)
ID=259 Latitude=32.2°N
ID=286 Latitude=47.75°S
ID=833 Latitude=56.5°N
ID=71 Latitude=41.28°S
ID=805 Latitude=70.3°N
ID=288 Latitude=64.15°N
ID=253 Latitude=41.50°N
Lunar declination (°)
2014-08-01
2014-08-31

C

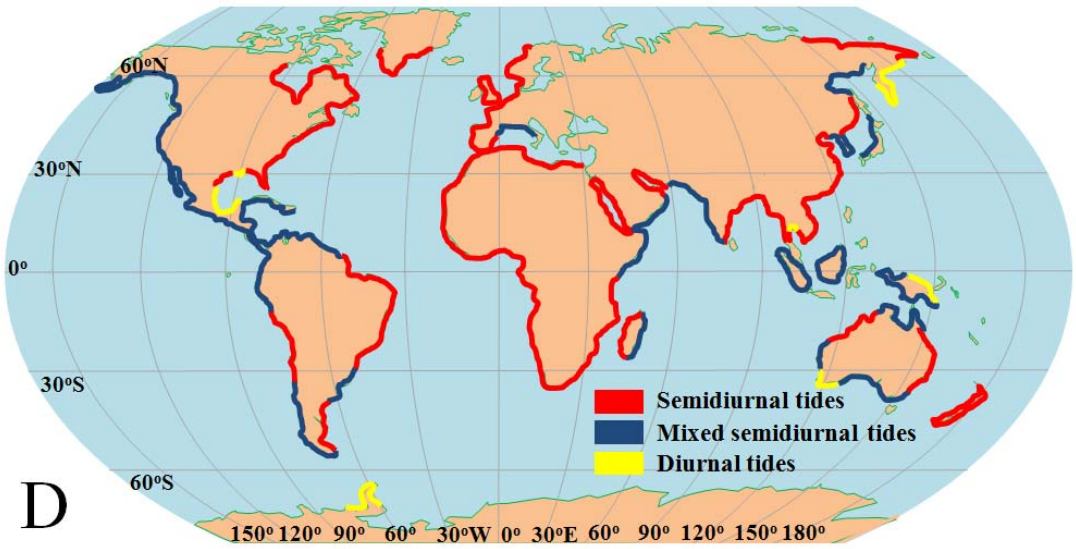

FIG. 1 Tidal bulges Versus Water Level Change. A, modelling the frame of two tidal bulges and the Moon in space. Area *a-cdef* and *b-ghij* denote the two bulges. *O* and *M* denote respectively the Earth's centre and the Moon's. θ is the lunar angle. Note that, the deformation is highly exaggerated; **B**, water level changes of 229 tide gauge sites out to their lunar angles in the day of August 13, 2014. Tide gauge data are extracted from GLOSS database-UHSLC (Caldwell et al. 2015): **C**, the evolution of high and low waters of the observed tides out to lunar declination in August, 2014. ID of each site refers to Table1; D, tidal pattern distribution of the observed tides throughout the globe. Data supporting is from U.S. NOAA, GLOSS database - UHSLC (Caldwell et al. 2015), and from Bureau National Operations Centre (BNOC) of Australia.

2 An analytic treatment of solid Earth deformation

The Earth may be treated as a solid sphere that is enveloped by water and atmosphere (Fowler 2004; National Research Council 1964, 1993). The structure of solid Earth, from surface to interior, is sequentially divided into different layers like crust, mantle, outer core, and inner core (Jordan 1979). A large number of works had confirmed that these layers are filled with various materials (Wootton 2006; Stixrude and Cohen 1995; Ozawa et al. 2011; Herndon 1980; Herndon 2005; Birch 1964) and denser materials are concentrated towards the interior (Monnereau et al. 2010). Notwithstanding, solid Earth is strictly not a rigid body. Both experiment and measurement had proved it to be

elastic (Stixrude and Cohen 1995; Schettino 2014) and to had been stretched into an oblate spheroid because of the centrifugal effect of the Earth's rotation about its axis (Heiskanen 1962; Burša 1993). It has been already established that there are two curved motions for the Earth in space: one is the Earth orbits about the centre of mass of the Earth-Moon system, and another is the Earth-Moon system orbits about the Sun. Fuller details of these motions of the Earth, Moon, and Sun may be found in these works (Kopal 1969; Schureman 1976; Smart 1940; Doodson and Warburg 1941; Kaula 1968; Roy 1978). These two curved motions generate two centrifugal effects F_1 and F_2 for solid Earth (Fig. 2(a_1)). F_1 and F_2 are mechanically balanced by the gravitation f_1 from the Moon and by the gravitation f_2 from the Sun. The ratio of F_1 and F_2 will be 1:178 according to some established parameters such as orbital radius and period, mass of each body, and so on. Apparently, F_2 is far greater than F_1, but as its working point is not at the Earth's centre, we need to suppose the effective part of F_2, which is able to stretch the Earth, to be relatively small and to exert at the Earth's centre. The counteraction of F_1 (F_2) and f_1 (f_2) elongates solid Earth along the direction of the Earth-Moon (Sun) line and compresses it in the midway of the elongation, the net effect is solid Earth becomes an oblate spheroid (Fig. 2(a_2 and a_4)). We call these lunar and solar deformations in the following sections. A rigorous dynamically treatment on this matter may refer to Pugh's work (1987, pp 60-63). We here employ hourly gravity data of 9 gauge sites from IGETS (International Geodynamics and Earth Tide Service) (Voigt et al., 2016) to examine this deformation of solid Earth. IGETS is the main data center of worldwide high precision superconducting gravimeter records, and the products hosted at the IGETS data centers include raw gravity and local pressure records, gravity and pressure data corrected for instrumental perturbations, and gravity residual after particular geophysical corrections. Gravity data we select here are treated as follows: gravity change of an Earthly site is the difference of the mean of all hourly gravity changes of this site during the whole August and the hourly gravity change. This eventually yields a same reference frame (gravity is zero) for these data to be compared together. As shown in Figure 3, these sites trend to perform a fall of gravity when their lunar angles fall into a phase of 0^o~45^o and 135^o~180^o,

whereas perform a rise of gravity when their lunar angles fall into a phase of 45°~135°. The fall (rise) of gravity geographically represents a rise (fall) of elevation relative to the Earth's centre. As these sites are scattered on several continents (African, European, North American, for instance), their timely response to gravity, if further coupled with Figure 1(A), well fits to a frame of the two bugles of solid Earth.

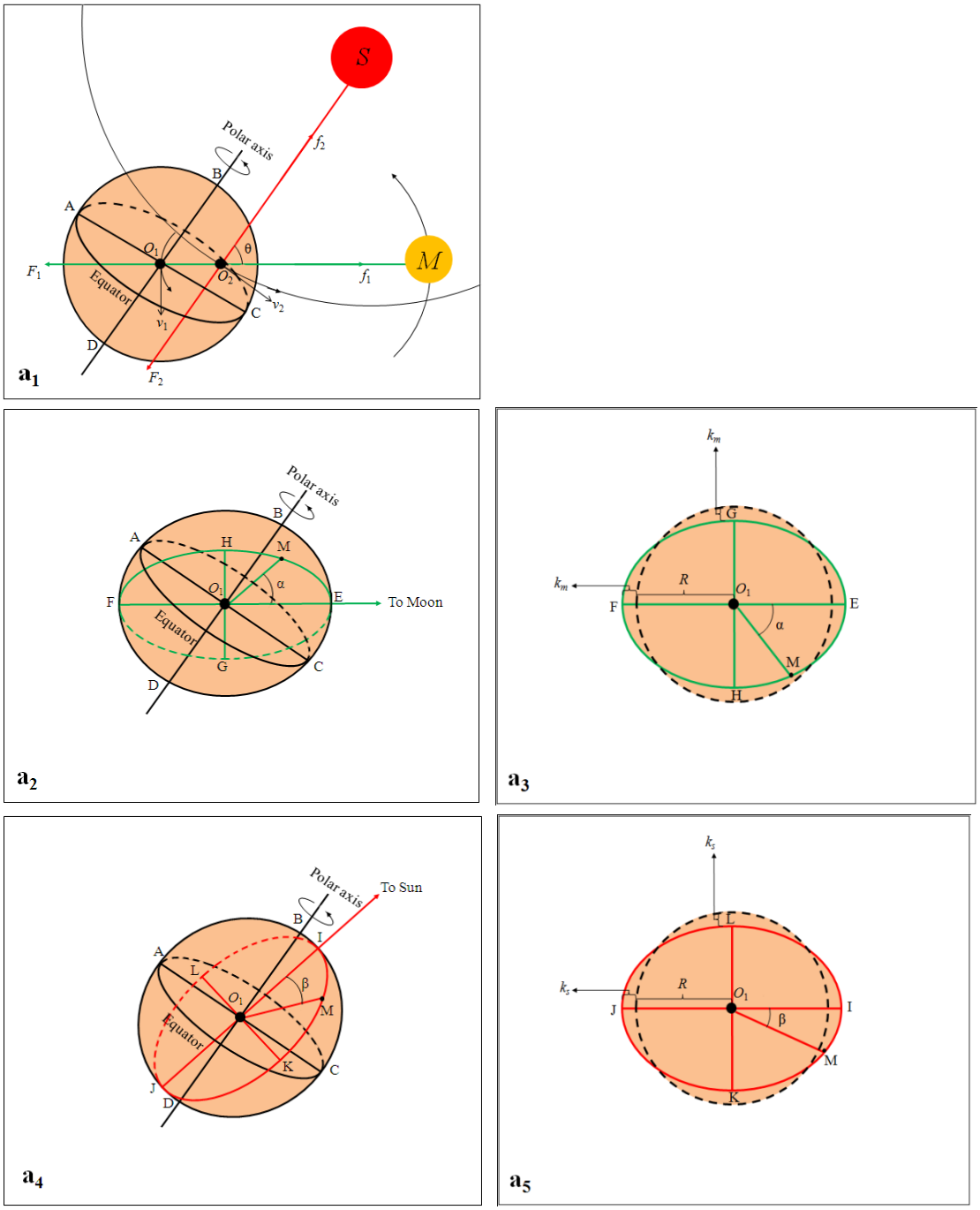

Fig. 2 Combined centrifugal effects for solid Earth and the resultant deformation. a_1, the curved motions of the Earth around the barycenter of the Earth-Moon system and around the Sun, a_2 and a_4 are the resultant deformations respectively from the Moon and from the Sun, a_3

and a_5 are the elliptical intersections respectively from these deformations. F_1 and F_2 are the centrifugal effects solid Earth undergoes due to these curved motions. O_1, O_2, M, and S are the Earth's centre, the barycenter of the Earth-Moon system, the Moon, and the Sun, respectively. Θ is the angle of the Moon and Sun relative to the barycenter of the Earth-Moon system. v_1 and v_2 are respectively the velocity of the Earth orbiting the barycenter of the Earth-Moon system and the velocity of the Earth-Moon system orbiting the Sun, it is these motions to generate the centrifugal effects F_1 and F_2. Black dashed circles in diagram a_3 and a_5 are referred as the original shape of solid Earth.

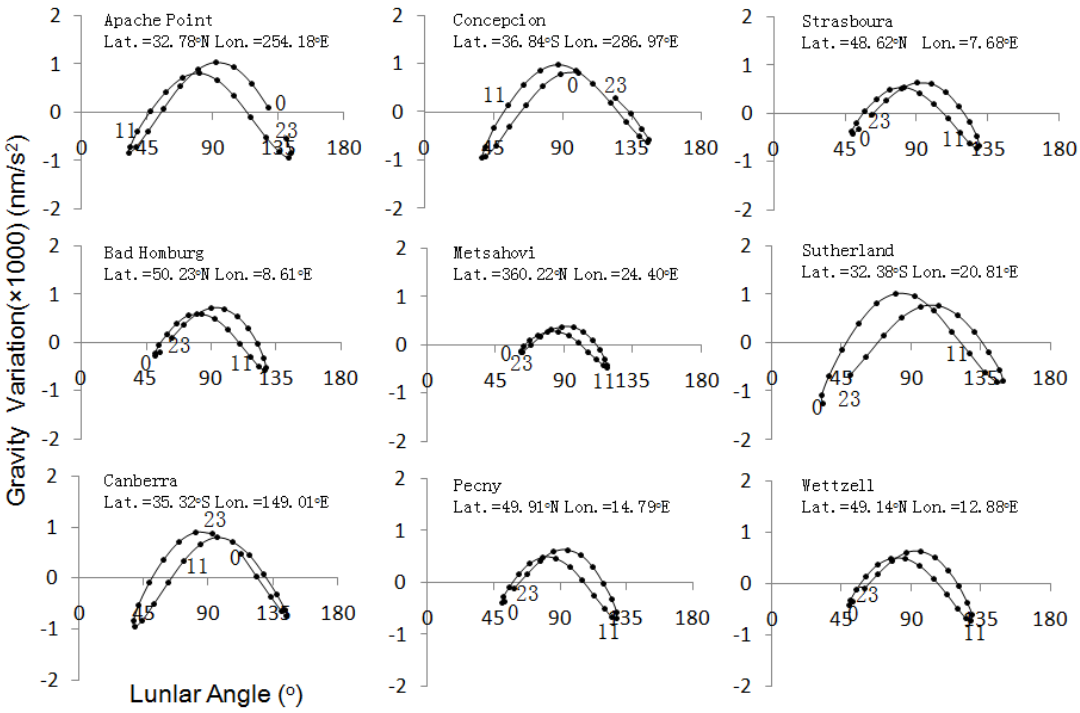

Fig. 3 Deformation of Solid Earth Versus Gravity Change. In each diagram number 0, 11, and 23 represent a GMT hour sequence of August 13, 2014. Hourly gravity data are extracted from IGETS (International Geodynamics and Earth Tide Service) (Voigt et al., 2016).

Solid Earth owns two sets of deformations at the same time, this determines that the distance of any Earthly site to the Earth's centre is a consequence of the combination of these two sets of deformations. Since a section which cuts an oblate spheroid along its long axis forms an ellipse (Fig. 3(a_3 and a_5)), and therefore, according to the geometry of ellipse, given some influences such as ocean tide loading and atmospheric loading,

earthquake, and storm events can be neglected, the vertical displacement of an Earthly site (marked with M) relative to the Earth's centre at time t may be expressed as

$$\Delta H_{(t)} = \Delta H(lunar)_{(t)} + \Delta H(solar)_{(t)}$$

$$\Delta H(lunar)_{(t)} = [(R+k_m)^2\cos^2\alpha + (R-k_m)^2\sin^2\alpha]^{1/2} - R$$

$$\Delta H(solar)_{(t)} = [(R+k_s)^2\cos^2\beta + (R-k_s)^2\sin^2\beta]^{1/2} - R \quad (1)$$

where $\Delta H(lunar)_{(t)}$ and $\Delta H(solar)_{(t)}$ are respectively the vertical displacement of site M in the lunar and solar deformations. R is mean radius of solid Earth, k_m and k_s denote the amplitude of the lunar and solar deformation. α and β are the lunar and solar angle of site M, they may be calculated through these formulas of spherical geometry: $\cos\alpha = \sin\sigma\sin\delta_m + \cos\sigma\cos\delta_m\cos C_{mm}$, $\cos\beta = \sin\sigma\sin\delta_s + \cos\sigma\cos\delta_s\cos C_{ms}$, where σ, δ_m, δ_s, C_{mm}, and C_{ms} are respectively the geographic latitude of site M, the declination of the Moon, the declination of the Sun, the hour angle of site M with respect to the Moon, and the hour angle of site M with respect to the Sun.

The expression above allows the assumption that the elongation and depression for each set of deformation stay equal in amplitude, and indicates that the vertical displacement $\Delta H_{(t)}$ is related to the angles α and β, this further means that site M would regularly rise and fall as the Earth spins. The amplitudes of the rise and fall vary with the adjustment of the relative positions of the Moon, Sun, and Earth, in particular, they becomes maximum at the times of full and new Moon and minimum at the times of first quarter and last quarter. This is because at the times of full and new Moon the two sets of deformations add each other to reinforce, whereas at the times of first quarter and last quarter the two cancel each other to weaken. The deformation amplitude $k_m(k_s)$ may be got from a relation of gravity and lunar angle. Gravitation acceleration at an Earthly site fits to an expression $g_H = GMe/H^2$, the resultant gravity change would be $\Delta g = (1/H^2 - 1/R^2)GMe$ when $g = GMe/R^2$ is referred, where G, Me, R, and H are respectively gravitation constant, mass of the Earth, mean radius of the Earth, and the distance of the site from the Earth's centre, which, refer to equation (1), may be further written as $H = [(R+k_m)^2\cos^2\alpha + (R-k_m)^2\sin^2\alpha]^{1/2} + [(R+k_s)^2\cos^2\beta + (R-k_s)^2\sin^2\beta]^{1/2} - R$. A purely experienced treatment for these two sets of deformations would be $k_m = E_mQ_m(\cos\delta_m + \cos\Theta)$ and $k_s = Q_s\cos\delta_s$, where E_m is

elliptical coefficient of the Moon's orbit and may be written as $E_m = R_{ME}^2/R_M^2$ (R_{ME} and R_M are respectively the mean distance of the Moon from Earth and the orbital radius of the Moon), this influences the gravitational force f_1 and the centrifugal effect F_1, Q_m and Q_s denote the amplitudes of the lunar and solar deformations, δ_m, Θ, and δ_s denote respectively the Moon's declination, the angle of the Moon and Sun, and the Sun's declination. After these parameters are packed together, we use a set of hourly gravity data of 4 sites from IGETS (International Geodynamics and Earth Tide Service) (Voigt et al., 2016), which cover the whole August of 2014, by means of a regression analysis, to get Q_m and Q_s. As every gravity gauge site involved has its own reference level g_{re} when measurement is operated, the gravity change of a site may be expressed as $\Delta g = (1/H^2 - 1/R^2)GMe - g_{re}$. The calculated and measured gravity changes are compared in Figure 4, the values of related parameters (G, Me, R, and R_{ME}, for instance) that bear these calculations and the results for Q_m, Q_s, and g_{re} are listed in Table 2.

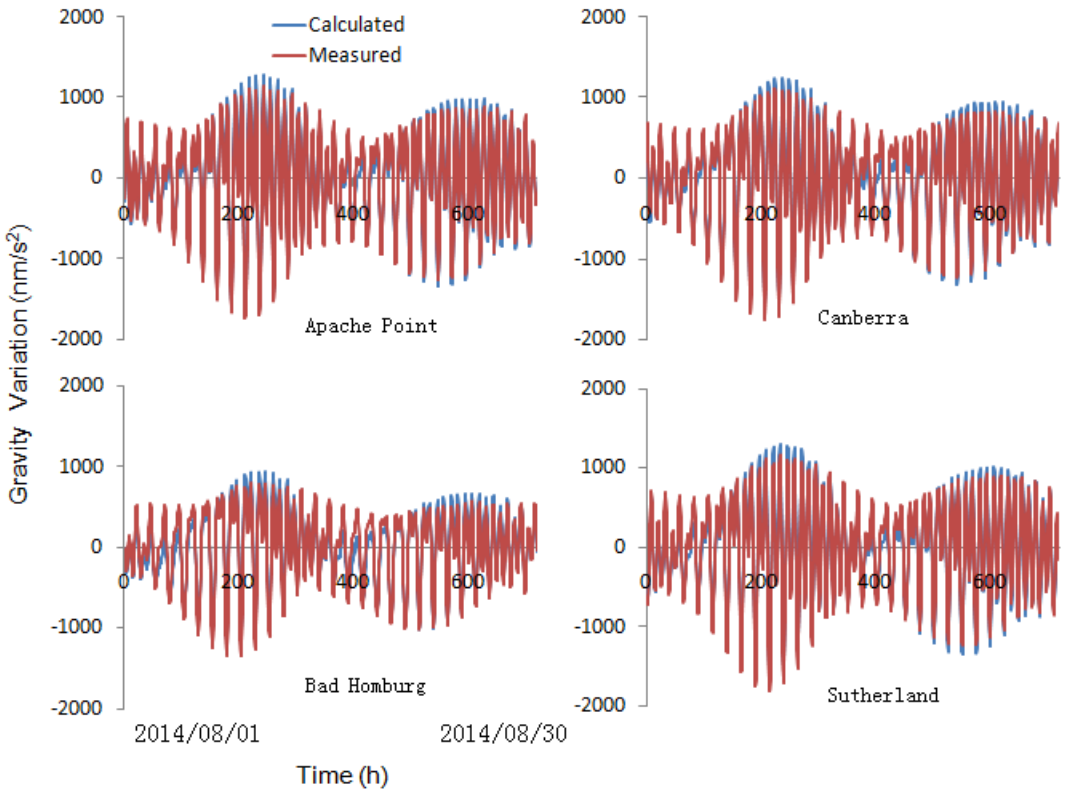

FIG. 4 Comparison of calculated and measured gravity change. Gravity data refer to IGETS (International Geodynamics and Earth Tide Service) (Voigt et al. 2016).

Table 2 Calculated results for lunar and solar deformations

Gravity gauge			Apache	Bad Homburg	Canberra	Sutherland	Mean
Q_m (m)			0.19	0.18	0.19	0.19	0.19
Q_s (m)			0.11	0.12	0.11	0.11	0.11
g_{re} (nm/s^2)			379.04	695.91	426.76	371.88	--
Astronomical parameters	Moon	M_m	$7.35*10^{22}$ kg (Wieczorek et al, 2006)				
		R_{ME}	384,400 km (Wieczorek et al, 2006)				
	Earth	M_e	$5.97*10^{24}$ kg (Luzum et al., 2011)				
		R	6370 km (Lide, 2000)				
	Sun	R_s	$1.49*10^{8}$ km (Simon et al., 1994)				
		M_s	$1.99*10^{30}$ kg (Williams, 2013)				
	G gravitational constant		6.67×10^{-11}m^{3}kg^{-1}s^{-2}				

Note: Q_m, Q_s, and g_{re} are respectively the amplitudes of the lunar and solar deformations, and gravity reference level of each site. M_m, M_e, and M_s are respectively the moon's, the earth's, and the sun's mass; R earth's mean radius, R_{ME} and R_s are respectively the mean distance of the moon from the earth and the mean distance of the sun from the earth.

3 An oceanic basin oscillation-driving mechanism for tide

3.1 Water movement in an oscillating vessel

Our understanding of tide begins with a demonstration of the water movement in an oscillating vessel. As shown in Figure 5, we firstly let the right end of a rectangular water box rise, the water then flows towards left. If line MN represents reference level, the water level at site M rises whereas the water level at site N falls. We restore the right end of the vessel to its former level and continue to let the left end rise, the water at the left end flows towards right, the water level at site M correspondingly falls whereas the water level at site N rises. Repeat the rise and fall of the two ends continuously, the water level of sites M and N alternately vary. Compared to sites M and N, another site S, which is located in the middle of this vessel, always holds a minimal variation of water level. Now we let only one end rise and fall alternately, the water level at sites M and N still alternately vary. Further, we let one end rise (fall) but another end fall (rise) at the

same time, the water level at sites M and N also alternately vary. The variation of water level at one end may be approximately expressed with a difference of vertical displacement between the two ends, i.e., $\Delta H=H_N-H_M$, where H_N and H_M denote respectively the vertical displacement of sites N and M. Mathematically, this variation may be depicted with a sinusoidal function *of* $h\sin(\omega t+\sigma)$, where h, ω, and σ denote respectively amplitude, angular frequency, and phase lag. Please note, this mode is different from the first gravitational mode of the oscillations of water that was mentioned in Pugh's work (1987, pp149), in that gravitational mode the vessel remains motionless and the oscillations of water are ascribed to a pull of the tide-generating force.

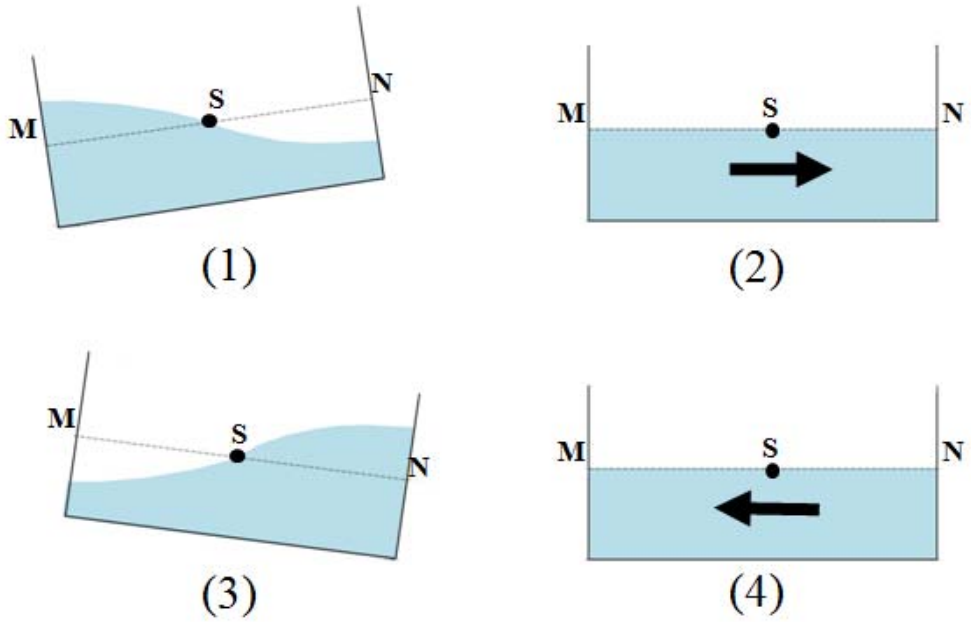

FIG. 5 Modelling the water movement of an oscillating rectangular box. From (1), (2), (3) to (4) it orderly represents a full alternation of the rise and fall of the two ends. Arrows denote the directions of water movements.

3.2 Ocean basin's oscillation and its resultant tide

About 71% the Earth's surface is covered with ocean (Pidwirny 2006), and each ocean basin looks like a gigantic vessel of water. Due to the existence of the two bulges of solid Earth, the spinning Earth drives each part of ocean basin to regularly move up

and down, this leads water to mechanically flow between all the parts of ocean basin. Refer to Figure 6, within the lunar deformation, the two bulges of solid Earth track from east to west along line *L* and *L'* as the Earth spins, this leads each part of ocean basin (i.e., *a*, *b*, and *c* may be some representative of infinite parts) to oscillate (i.e., rise and fall). These oscillations of ocean basin subsequently yield water movements between all the parts of the basin. Some factors influence water movements over the Earth's surface. The Coriolis force deflects the travelling water to right in the northern hemisphere and to left in the southern hemisphere. For example, the red lines a_1 and a_2 may represent real paths of the water movements from site *a* to site *b* and to site *c*, respectively. From deep oceans to shelf seas, the slope of sea floor greatly disperses and refracts the travelling water. In addition, the travelling water also would encounter continents, by which a reflection of water is formed. A more detailed treatment of the water movement around a rotating Earth refers to Laplace's hydrodynamic equations (Pugh 1987; Pugh and Woodworth 2014). The inflow of water at a site generates an increase of water level, whereas the outflow of water at a site generates a decrease of water level, and therefore, the inflow and outflow of water generate high and low water variation for each part of ocean basin. As ocean basin is separately oscillated by the two bulges of solid Earth, this ultimately gives each part of ocean basin two high waters and two low waters per day. If this oscillation of ocean basin that is generated due to the lunar deformation is connected to another oscillation of ocean basin that is generated due to the solar deformation, the composition of the resultant two sets of water movements becomes strongest at the times of full and new Moon and weakest at the times of first quarter and last quarter, this generates two cycles of high and low waters during a month. As water level variation of a site is associated with the water level variations of all sites, along with the influences of these factors (Coriolis force, the shape of ocean basin, for instance), these generate diversity for the times of high and low waters of all the sites around the globe.

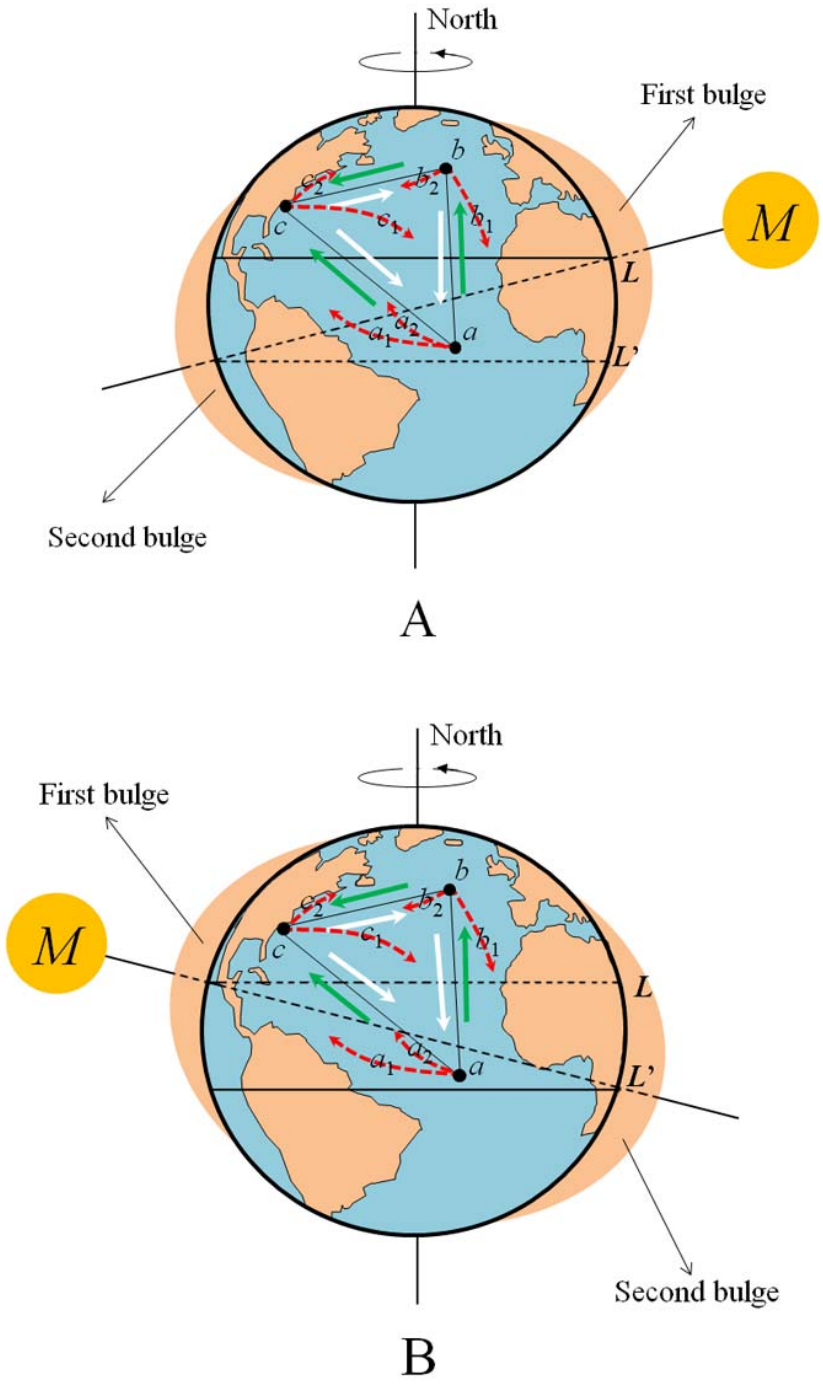

FIG. 6 A simplified system illustrates the spinning deformed solid Earth. From A to B, the Earth rotates 180° with respect to the Moon. *L* and *L'* denote the paths that the Earth-Moon line tracks along the Earth's surface (dashed line means it is at far side), the two bulges represent the elongation of solid Earth. *a*, *b*, and *c* are the representatives of infinite sites located in ocean basin, green and white arrows between them represent water movements along the horizontal direction.

3.3 Modelling

The demonstration above leads to a fact that, although water movements perform in an extremely complicated manner, from a viewpoint of globally water conservation, the water level variation of a site is always determined by the water level variations of all other sites within ocean basin. This provides a theoretical basis for us to account for the observed tide. To facilitate the following deduction, we divide ocean basin of the globe into a grid of 15^o*15^o and use the locations of nodes of the grid, which are situated in ocean basin, to act as oscillators (Figure 7), and then, the water level variation of a site at time t may be approximately expressed as

$$\Delta Y_{(t)} = \sum_{i=1}^{n}\sum_{j=1}^{k} Qa_ib_j\left(lunar\right)\Delta Ha_ib_j\left(lunar\right)_{(t)} + \sum_{i=1}^{n}\sum_{j=1}^{k} Qa_ib_j\left(solar\right)\Delta Ha_ib_j\left(solar\right)_{(t)}$$
$$+Q_s\left(lunar\right)\Delta H_s\left(lunar\right)_{(t)} + Q_s\left(solar\right)\Delta H_s\left(solar\right)_{(t)} \qquad (2)$$

where $\Delta Ha_ib_j(lunar)_{(t)}$ and $\Delta Ha_ib_j(solar)_{(t)}$ are respectively the vertical displacement of a_ib_j oscillator in the lunar and solar deformations at time t, n=24 and k=11, referring to the map, combine together to represent the number of oscillators. $\Delta H_s(lunar)_{(t)}$ and $\Delta H_s(solar)_{(t)}$ are respectively the vertical displacement of the site itself in the lunar and solar deformations at the time. These vertical displacements may be got from equation (1). $Qa_ib_j(lunar)$, $Qa_ib_j(solar)$, $Q_s(lunar)$, and $Q_s(solar)$ are the coefficients of oscillations of all related sites.

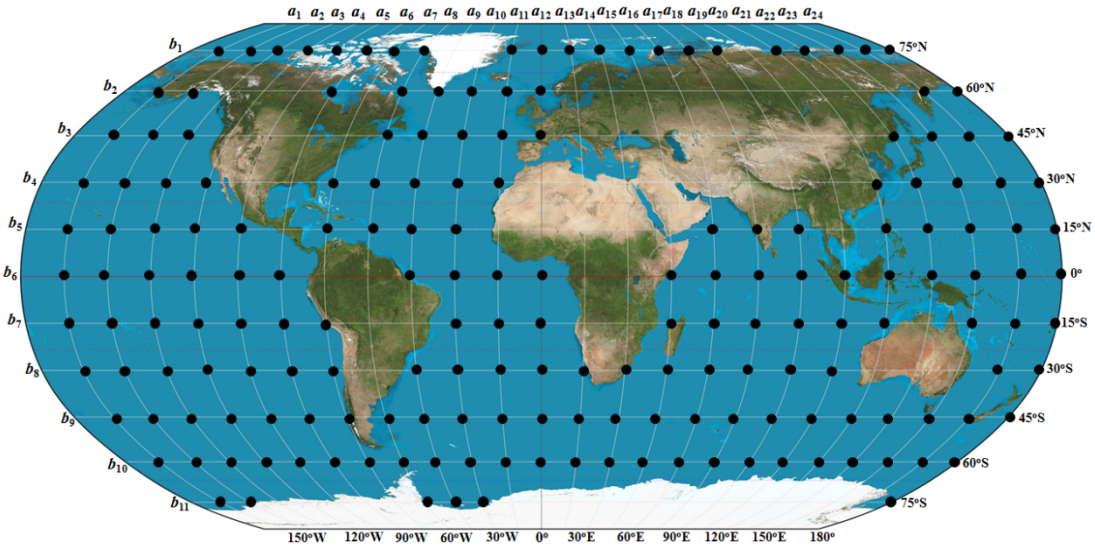

FIG. 7 Globally-distributed oscillators within ocean basin. The background image is created by Daniel R. Strebe with the Geocart map projection software.

About 187 oscillators are extracted from the nodes of the grid that covers ocean basin, the grid is plotted referring to both equator and meridian, this makes the geographic latitude and longitude of these oscillators easily known from the map. The behaviour of these oscillators is similar to that of the constituents of the harmonic analysis. The hourly tide-gauge data lasting the whole August of 2014 from 75 UHSLC stations and Karumba of Australia are used to test the model. The evaluation of the results is realized in term of the Root Mean Square (*RMS*) of amplitude. The *RMS* deviation for a tide-gauge site during the month may be written as

$$RMS = \sqrt{\frac{\sum_{i=1}^{m}\left(\Delta Y_{(t)-\mathrm{mod}elled} - \Delta Y_{(t)-observed}\right)^2}{m}} \tag{3}$$

where $\Delta Y_{(t)\text{-}modelled}$ and $\Delta Y_{(t)\text{-}observed}$ denote respectively the in-phase amplitudes of the modelled and tide-gauge data, and m=744, which denotes a time sequence of 31 days multiply 24 hours during the month.

The results for these 76 tide-gauge stations are listed in Table 3, some of the modelled results and tide-gauge data are also compared in Figure 8. These fittings strongly agree that the observed tide may be a consequence of the oscillation of ocean basin.

The model presented here may be used to make tide prediction. Simply, it firstly takes the tide-gauge data by a regression analysis to solve the coefficients of all oscillations involved, and then, each of these coefficients are further used to multiply the vertical displacement of its corresponding oscillation at the future time, a tidal height for each oscillation is therefore got, subsequently, a simple addition of these tidal heights gives the total tidal height at the location at the future time. We take the hourly tide-gauge data covering the whole August of 2014 to make tidal prediction in the following month (September 2014) and find that the prediction is successful for some of the 76 sites we selected above. Figure 9 compares the tide predictions of four sites (Atlantic city, San Francisco, Adak, and Betio) with the observations. The evaluation of these

predictions is made through the Root Mean Square (*RMS*) to estimate the average errors. The calculated *RMS*s for these sites are 16.36, 15.47, 16.79, and 19.78 cm, respectively.

The improvement of this model and its resultant prediction should be focused on two aspects: 1) ocean basin may be divided into smaller grid of 5^o*5^o or 1^o*1^o, this may help to add more oscillators into the model. We believe, more oscillators the model holds, more accurate the model would become. It is also important to note, a well-equipped computer and powerful software should be prepared for the addition of more oscillator. This model uses a computer of CPU 3.40 GHz and RAM 16.0 GB with a software (1stOpt-First Optimization, 7.0 version) to calculate, but not too satisfactory, each round of regression analysis takes too much time; and 2) a longer tide-gauge data of a few months or one year should be considered to resolve the coefficients of oscillations of the model so as to enhance the accuracy of tide prediction. A merit of this model is the time lag of tide is unnecessary to be considered.

Table 3 RMS calculated for 76 sites over different regions

Tide-gauge station					RMS (cm)
ID at UHSLC	Name	Latitude	Longitude	Region	
1	Betio (Tarawa)	1.35	172.92	D	6.87
3	Baltra	0.43	269.72	D	16.10
5	Majuro	7.10	171.37	D	9.06
7	Malakal	7.33	134.47	D	7.02
8	Yap	9.52	138.13	D	6.43
14	French Fr Shall	23.87	193.72	D	3.21
15	Papeete	-17.53	210.43	D	2.36
16	Rikitea	-23.13	225.05	D	4.65
22	Easter	-27.15	250.55	D	7.30
23	Rarotonga	-21.20	200.22	D	4.79
24	Penrhyn	-8.98	201.95	D	2.80
29	Kapingamarangi	1.10	154.78	D	4.41
31	Nuku	-8.93	219.92	D	8.97
38	Nuku' alofa	-21.13	184.83	D	8.26

39	Kodiak	57.73	207.48	S	15.73
40	Adak	51.87	183.37	S	9.60
41	Dutch	53.90	193.50	S	12.78
43	Palmyra	5.87	197.90	D	3.67
46	Port Vila	-17.77	168.30	D	4.74
47	Chichijima	27.10	142.18	S	3.75
49	Minamitorishima	24.30	153.97	D	9.03
50	Midway	28.22	182.63	D	3.16
51	Wake	19.28	166.62	D	4.12
52	Johnston	16.75	190.48	D	2.99
53	Guam	13.43	144.65	D	3.81
55	Kwajalein	8.73	167.73	D	5.07
56	Pago	-14.28	189.32	D	6.04
58	Nawiliwili	21.97	200.65	D	3.02
60	Hilo	19.73	204.93	D	3.78
71	Wellington	-41.28	174.78	D	11.72
72	Bluff	-46.60	168.33	D	15.78
79	Chatham	-43.95	183.43	D	9.76
80	Antofagasta	-23.65	289.60	SC	7.14
81	Valparaiso	-33.03	288.37	SC	7.62
83	Arica	-18.47	289.67	SC	7.38
88	Caldera	-27.07	289.17	SC	7.56
91	La	-2.20	279.08	SC	9.87
93	Callao	-12.05	282.85	SC	5.25
94	Matarani	-17.00	287.88	SC	5.38
101	Mombasa	-4.07	39.65	SC	14.05
103	Port Louis	-20.15	57.50	SC	3.96
105	Rodrigues	-19.67	63.42	D	4.60
108	Hulhule	4.18	73.53	D	3.78
109	Gan	0.68	73.15	D	4.04
115	Colombo	6.97	79.87	SC	3.51
119	Djibouti	11.60	43.15	SC	7.60
121	Point La Rue	-4.67	55.53	D	6.40
122	Sibolga	1.75	98.77	SC	4.81
124	Chittagong	22.23	91.83	SC	39.57

125	Prigi	-8.28	111.73	SC	8.70
126	Jask	25.63	57.77	SC	10.46
128	Thevenard	-32.15	133.63	SC	15.61
142	Langkawi	6.43	99.75	SC	7.64
147	Karachi	24.80	66.97	SC	12.71
149	Lamu	-2.27	40.90	SC	11.77
211	Ponta Delgada	37.73	334.32	SC	6.90
223	Dakar	14.70	342.60	SC	7.24
235	Palmeira	16.70	337.00	D	4.09
245	San Juan	18.47	293.88	SC	3.32
253	Newport	41.50	288.67	SC	9.49
257	Settlement Point	26.72	281.00	SC	6.60
259	Bermuda	32.37	295.30	D	7.42
260	Duck Pier	36.18	284.27	SC	9.66
264	Atlantic City	39.40	285.00	SC	10.73
276	St-John's	47.57	307.28	SC	7.91
299	Qaqortoq	60.70	314.00	SC	14.77
329	Quarry Bay	22.30	114.22	SC	9.00
340	Kaohsiung	22.62	120.28	SC	5.53
540	Prince Rupert	54.32	229.67	SC	26.88
551	San Francisco	37.80	237.53	SC	9.70
752	Fort Pulaski	32.03	279.10	SC	18.35
755	Virginia Key	25.70	279.90	SC	7.38
776	Punta Cana	18.50	291.62	SC	3.05
803	Rorvik	64.87	11.25	SC	11.31
820	Nuuk	64.17	308.28	SC	20.62
*	Karumba	-17.7	139.2	SC	24.00

Note: D, Deep ocean; SC, Shelf and Costal area. Karumba isn't included in UHSLC.

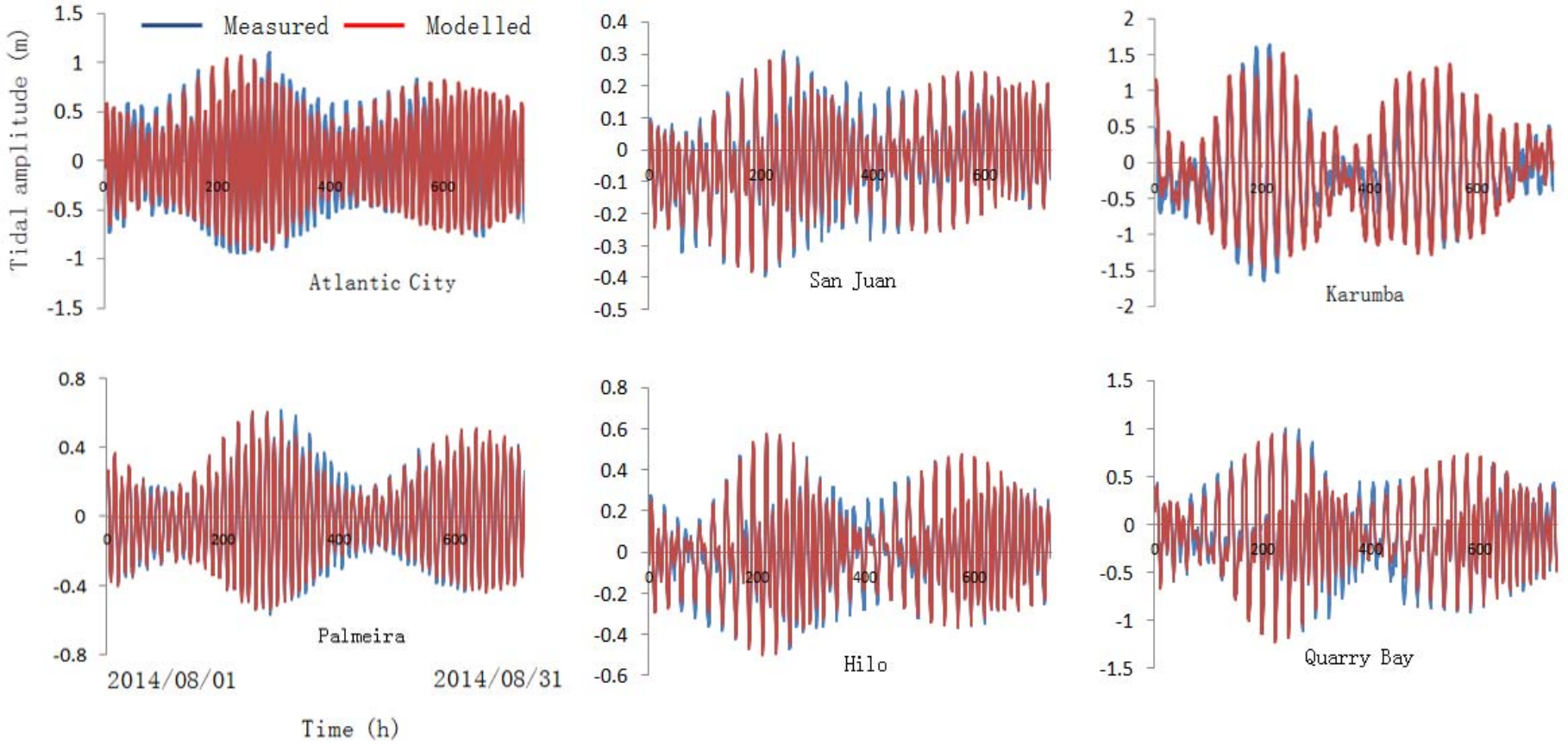

FIG. 8(A) Representatives of the comparison between the modelled and tide-gauge data covering the whole August of 2014.

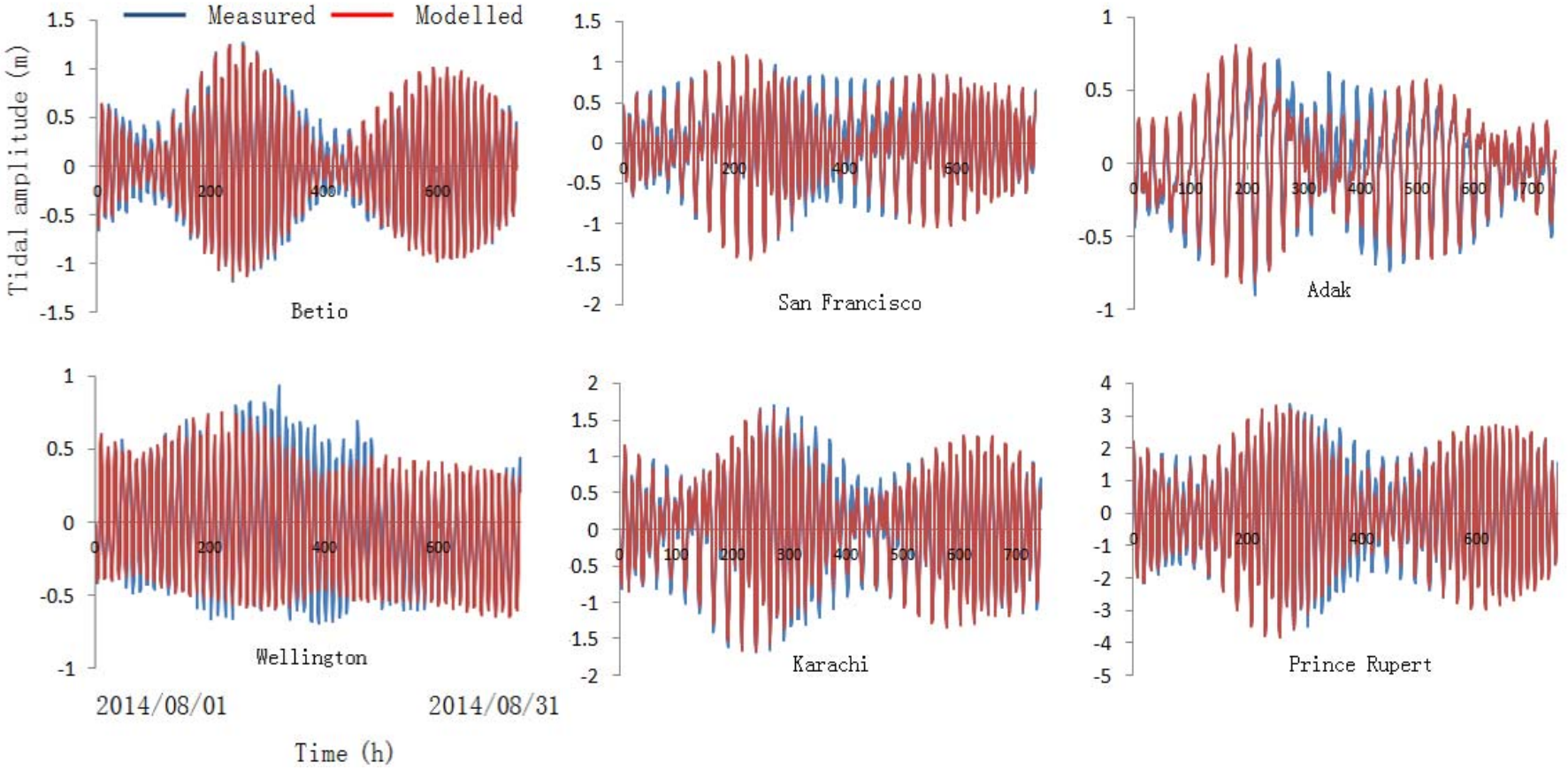

FIG. 8(B) Representatives of the comparison between the modelled and tide-gauge data covering the whole August of 2014.

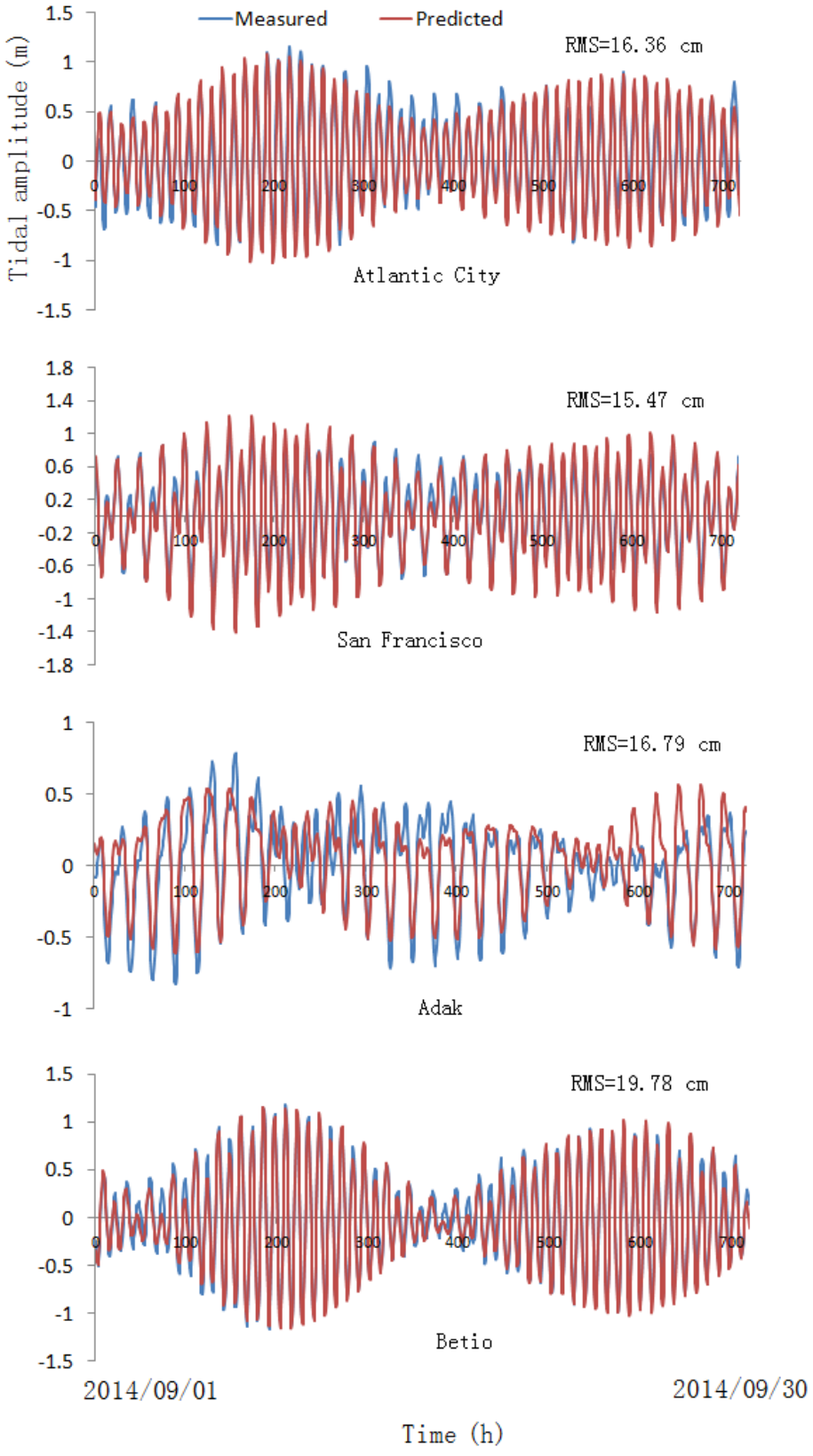

FIG. 9 A comparison of the predicted and tide-gauge data over the whole September of 2014.

4 Discussion

The tide modelling presented here shows that the observed tides may be a consequence of the oscillation of ocean basin, but this realization doesn't exclude other way to yield the observed tides. For example, many of the established tide models had successfully yielded the observed tides (Shum et al. 1997; Stammer et al. 2014). Also, we have shown in section 1.2 that the Moon's gravitational attraction hasn't formed a pair of water bulges on the Earth's surface, but it is unclear whether the Moon's gravitational attraction drives ocean or not, an exploration on this issue is still needed. Following the line we presented above, some clarifications on related subjects need to be made further.

4.1 Problem of the established tidal theory

The established tidal theory may be divided into two parts: the equilibrium tide, which is represented with the two bulges of water, and the dynamic tide. The equilibrium tide, as demonstrated earlier, is a net result of the attractive mechanism. According to these authors (e.g., Pugh 1987; Pugh and Woodworth 2014), the dynamic tide was formed based on a consideration of the influences of several factors such as continent, seafloor topography, and the Earth's rotation. An earlier treatment of this matter was made by Laplace who expanded the equilibrium tide into a set of hydrodynamic equations of continuity and momentum. Laplace assumed spherical earth to be with a geocentric gravitational field, a rigid ocean bottom, and a shallow ocean, which allowed Coriolis accelerations to be neglected. These equations are further followed by a series of ideas such as standing wave, resonance, Kelvin wave, amphidromic system, and so on (Pugh 1987; Pugh and Woodworth 2014). Based on these theoretical ideas, the tides in the oceans and continental shelf seas are generally explained. For example, in the Pacific ocean the dominant tides are semidiurnal, these tides are well consistent with the amphidromes proposed to exist respectively at 25^{o} N, 135^{o} W and near 25^{o} S, 150^{o} W. Such amphidrome gives very small M_2 tides in the vicinity of the Society Isles (Pugh 1987); In the Atlantic ocean small tides are observed, these tides suggest a tendency for an amphidromic system to develop. The ranges become relatively large near equator and the phase is nearly constant over an extensive area, high waters occur along the whole coast of northern Brazil from 35^{o} W to 60^{o} W within an hour, this behaviour is consistent with standing wave dynamics. The most fully developed semidiurnal amphidrome is located near 50^{o} N. The tidal wave seems to travel round the position in a form which approximates to a Kelvin

wave (Cartwright et al. 1980; Schwiderski 1979; Pugh 1987); In the north-west European continental shelf, the tides are thought to be derived from co-oscillation with the Atlantic Kelvin wave, the largest amplitudes occur when the Kelvin wave moves along the British coast (Proudman and Doodson 1924; Sager and Sammler 1975; Huntley 1980; Howarth and Pugh 1983; Pugh 1987; Pugh and Woodworth 2014).

Undoubtedly, explaining tide should be wider, it includes not only telling the reason why there are tides (i.e., the daily and fortnightly cycles of high and low water) but also telling how tidal patterns (i.e., semidiurnal, diurnal) distribute and why there are tidal range differences between ocean and shelf sea. Nevertheless, in the long history of tide, most of people preferred to go after the reason why there are tides, although the issues of tidal pattern distribution and tidal range difference are still important especially when some practice activities like shipping and sea exploration are related. On the whole, the equilibrium tide is taken to explain why there are tides, while the dynamic tide is taken to explain how tidal patterns distribute and how tidal range difference occurs, as that are shown above. Subsequently, as we concluded in section 1.2, without the two bulges of water, the reason why there are tides would become unresolved in the established tidal theory. In contrast, the oceanic basin oscillation-driving mechanism presented gives the answer.

4.2 Ocean tide models

Ocean tide models generated after both tide-gauge data and satellite altimeter data had been collected, they are of course the need for geophysical corrections in the fields such as oceanography and space technology (Provost 1994). The first generation of ocean tide models appeared between 1960's and 1980's and followed by improved works in the following decades. Ocean tide models include modern data-constrained models such as GOT4.8 (Ray 1999) and TPXO8 (Egbert and Erofeeva 2002), purely hydrodynamic models such as HIM (Arbic et al. 2008), OTIS-ERB (Egbert et al. 2004), and STM-1B (Hill et al. 2011), and historic data-unconstrained models such as NSWC (Schwiderski 1979) and CSR3.0 (Eanes and Bettadpur 1996). Some comprehensive evaluations of these models may refer to these two works (Shum et al. 1997; Stammer et al. 2014). Nowadays, most of tides around the world may be got through these models. Ocean tide models are essentially a consequence of the combination of computer and empirical technique. In these models, many different variables can be

packed together to be treated, moreover, the time of data processing is greatly shortened, these totally allow the decomposed components more reliable and exact.

There are differences between these established tide models and the ocean basin oscillation model presented here. On the one hand, most of these established models are characterized by a network of smaller grids plotting oceans and use the elevation of ocean to synthesize the observed tides, while this model cuts ocean basin into a network of smaller grids and uses the elevation of basin to synthesize the observed tides. On the other hand, these models employed various frequencies (notably M_2, S_2, N_2, K_2, K_1, O_1, P_1, and Q_1, for instance), while the frequencies of this model are constant, which are equal to that of M_2 and S_2. These differences determine that we cannot use this model to make comparison with these established models.

It is necessary to differentiate this ocean basin oscillation model from the resonant ocean oscillation model. R.A. Harries firstly considered ocean as a resonantly oscillating system, Platzman (1975) provided a theoretical basis for the understanding, i.e., for a basin of depth h and horizontal length l, the resultant oscillating frequency is $2l/(gh)^{1/2}$, where g is the gravitational constant. Platzman, however, didn't use this kind of resonant oscillation to directly get the observed tides, instead, he used normal modes to synthesize the observed tides (Platzman 1978; 1983; and 1984). Moreover, Platzman's modes employed various frequencies, and some of the frequencies are very close to those of some of the main constituents (notably K_1), while the frequencies of this model are constant.

4.2 Tidal prediction

Many people (especially those engage in tidal field) mistakenly attribute the success of tidal prediction to the attractive mechanism. Before this work is put forward further, we need to clear out this misconception. A widely accepted routine for tidal prediction is by means of tide observation. As tidal variations (the height and time of high and low waters) are recorded continuously, once tide data become available, one may use computers to analyze the data to identify many components of complex wave. Tidal analysis usually employs three methods: non-harmonic, harmonic, and responsive. A detailed description of these methods may refer to the Pugh's work (1987). Historically, William Thomson devised the harmonic method about the year 1867. The principle of this method is that any periodic motion or oscillation can always be resolved into the sum of a series of simple harmonic motions. Apparently, a curve plotted from tide record may be regarded as a complex wave. As wave has crest and trough, this feature

corresponds to the high and low water of a tide. Harmonic analysis makes full use of this point, by which the tidal variations (high and low) are represented with a finite number of harmonic terms of cosine form ($H_n\cos(\sigma_n t - g_n)$, where H_n is amplitude, g_n is phase lag, and σ_n is angular speed). Tidal analysis worked out the wave heights and time lags (related to the Moon's or Sun's orbital movement) of many components. Once the timing, periodicity, and amplitude of each component are known for a particular location, a simple addition of these components gives the tidal height at the future time at the location. In other words, by the harmonic method the decomposed tide components are finally recombined into a composite tide. Tidal predictions made in this way are used extensively and give the basis for the tide forecasts we daily see in many public forms (Segar 2012). These arguments lead to the fact that tidal prediction is irrelevant to the attractive mechanism. The tidal prediction presented in section 3 further supports that the methods for making tidal prediction may be various, no limited to the classical harmonic method.

4.3 Earth tide

Solid Earth deformation (also called Earth tide) was firstly presented by Love (1909), Longman (1963) introduced a Green's function, by which Earth tide can be calculated exactly, these authors (Hendershott 1972; Farrell 1973; Melchior 1974; Agnew 1981; Scherneck 1991) systematically investigated the responses of solid Earth to the tide-generating forces and to ocean tide. The currently view is that the impact of Earth tide on ocean tide may be expressed with $(1+k-h)\Omega p/g$, where $\Omega p/g$ is the equilibrium tide amplitude, $(1+k-h)$ is a diminishing factor (combination of Love numbers) in the equilibrium tide (Pugh 1987; Pugh and Woodworth 2014). This treatment, however, lost something important. Since $(1+k-h)\Omega p/g$ itself represents that the contribution of Earth tide to ocean tide is simply a reduction of tide amplitude, this reduction requires the occurrence of Earth tide and the occurrence of ocean tide to be synchronous. This work shows that, as inferred from Figure 1 and Figure 3, both Earth tide and ocean tide are not synchronous, this results in that one cannot get the observed through a reduction of Earth tide from ocean tide.

The results of solid Earth deformation may be influenced by several factors. On the one hand, near-surface geology may yield local anomalies while responding to the tidal forcing. On the other hand, the loading/unloading of ocean tide may lead the Earth's lithosphere to vertically displace and become tilt (Farrell 1973; Pugh 1987).

Additionally, atmospheric loading and some extreme events such as storm and earthquake would also exert effect on the Earth's lithosphere.

4.4 Application of ocean basin oscillation

The physics of ocean basin oscillation is also applicable to the matter of an enclosed sea/lake. If we treat Black sea as a vessel and use equation (1) presented in section 2 to estimate, the west or east end of this region may experience a tide of up to 17.0 cm. Similarly, a tube of water (20 m in length) horizontally located at equator would experience a tide of up to $3.2*10^{-3}$ mm, an imperceptible amount. This means that, any smaller vessel, such as swimming pool, cup, bowl, and so on, because of its short size, wouldn't exhibit a perceptible tide.

Acknowledgements We particularly thank Phil Woodworth and John Huthnance for their suggestive comments on this work, and thank Walter Babin, Thierry De Mees, Roger A. Rydin, and Wouter Schellart for the reviews on the original manuscript, thank Hartmut Wziontek and Calvo Marta for discussions on gravity data, and thank Mike Davis for providing tide data. We also thank these institutes (U.S. NOAA, NASA's JPL, GLOSS database - University of Hawaii Sea Level Center, Bureau National Operations Centre (BNOC) of Australia, and GGP (Global Geodynamics Project)) for their data supporting.

References

Agnew, D. C., 1981. Nonlinearity in rock - Evidence from Earth tides. J. geophys. Res. 86, 3969-3978.

Arbic, B. K., J. X. Mitrovica, D. R. MacAyeal, and G. A. Milne, 2008. On the factors behind large Labrador Sea tides during the last glacial cycle and the potential implications for Heinrich events. Paleoceanography. 23, PA3211, doi:10.1029/2007PA001573.

Birch, F., 1964. Density and Composition of Mantle and Core. Journal of Geophysical Research Atmospheres. 69(20), 4377-4388.

Bowman, M. J., A. C. Kibblewhite, R. A. Murtagh, S. M. Chiswell, B. G. Sanderson, 1983. Circulation and mixing in greater Cook Strait, New Zealand. Oceanol. Acta. 6(4), 383-391.

Burša, M., 1993. Parameters of the Earth's tri-axial level ellipsoid. Studia Geophysica et Geodaetica. 37(1), 1-13.

Caldwell, P. C., Merrfield, M. A., Thompson, P. R., 2015. Sea level measured by tide gauges from global oceans - the Joint Archive for Sea Level holdings (NCEI Accession 0019568). Version 5.5, NOAA National Centers for Environmental Information, Dataset, doi:10.7289/V5V40S7W.

Cartwright, D. E., Edden, A. C., Spencer, R., Vassie, J. M., 1980. The tides of the northeast Atlantic Ocean. Philosophical Transactions of the Royal Society of London. A298, 87-139.

Cartwright, D. E., R.Spencer, F.R.S., Vassie, J. M., Woodworth, P. L., 1988. The tides of the Atlantic Ocean, 60°N to 30°S. Philosophical Transactions of the Royal Society of London. 324, 513-563.

Cartwright, D. E., 1999. Tides: A Scientific History. Cambridge University Press.

Deacon, M., 1971. Scientists and the Sea, 1650-1900. Academic Press (London).

Defant, A., 1961. Physical Oceanography. Volume II. Oxford: Pergamon Press, 598 pp.

Doodson, A. T., Warburg, H. D., 1941. Admiralty Manual of Tides. London HMSO.

Eanes, R., Bettadpur, S., 1996. The CSR 3.0 global ocean tide model. Tech. Memo. CSR-TM-96-05, Center for Space Res., Univ. Texas, Austin.

Egbert, G. D., Erofeeva, S. Y., 2002. Efficient inverse modeling of barotropic ocean tides. J. Atmos. Oceanic Tech. 19, 183-204.

Egbert, G. D., Ray, R. D., and Bills, B. G., 2004. Numerical modeling of the global semidiurnal tide in the present day and in the last glacial maximum. J. Geophys. Res. 109, C03003, doi:10.1029/2003JC001973.

Farrell, W. E., 1973. Earth tides, ocean tides and tidal loading. Philosophical Transactions of the Royal Society of London. A274,253-259.

Fowler, C. M. R., 2004. The Solid Earth: An Introduction to Global Geophysics (2nd Education). Cambridge University Press.

Fu, L. -L., Cazenave, A., 2001. Satellite Altimetry and Earth Sciences. Academic Press, San Diego, Calif.

Gao, Z. Z., He, Y. B., Li, X. D., Duan, T. Z., 2013. Review of research in internal-wave and internal-tide deposits of China. Journal of Palaeogeography. 2 (1), 56-65.

Gargett, A. E., Hughes, B. A., 1972. On the interaction of surface and internal waves. Journal of Fluid Mechanics. 52, 179-191.

Garrett, C., Munk, W., 1979. Internal waves in the ocean. Annual Review of Fluid Mechanics. 1, 339-369.

Heiskanen, W. A., 1962. Is the Earth a triaxial ellipsoid?. J. geophys. Res. 67 (1), 321-327.

Hendershott, M. C., 1972. The effects of solid Earth deformation on global ocean tides. Geophysical Journal of the Royal astronomical Society. 29, 389-402.

Herndon, J. M., 1980. The chemical composition of the interior shells of the Earth. Proc. R. Soc. Lond.. A372(1748), 149-154.

Herndon, J. M., 2005. Scientific basis of knowledge on Earth's composition. Current Science. 88(7), 1034-1037.

Hill, D. F., Griffiths, S. D., Peltier, W. R., Horton, B. P., and Tornqvist, T. E., 2011. High-resolution numerical modeling of tides in the western Atlantic, Gulf of Mexico, and Caribbean Sea during the Holocene. J. Geophys. Res. 116, C10014, doi:10.1029/2010JC006896.

Howarth, M. J., Pugh, D. T., 1983. Observations of tides over the continental shelf of northwest Europe, pp. 135-85, in Physical Oceanography of Coastal and Shelf Seas (ed. B. Johns). Amsterdam: Elsevier, 470 pp.

Huntley, D. A., 1980. Tides on the north-west European continental shelf. In The North West European Shelf Seas: the Sea Bed and the Sea in Motion. II. Physical and Chemical Oceanography, and Physical Resources (ed. F. T. Banner, M. B. Collins and K. S. Massie). Amsterdam: Elsevier, pp. 301-51.

Jordan, T. H., 1979. Structural Geology of the Earth's Interior. Proc. Natl. Acad. Sci. USA. 76 (9), 4192-4200.

Kaula, W. M., 1968. Introduction to Planetary Physics: the Terrestrial Planets. John Wiley.

Kopal, Z., 1969. Dynamics of the Earth-Moon System. Springer Netherlands.

Lamb, H., 1932. Hydrodynamics. 6th edn. Cambridge University Press, 738 pp.

Lambeck, K., 1988. Geophysical Geodesy. Clarendon Press, Oxford.

Lide, D. R., 2000. Handbook of Chemistry and Physics (81st ed.).

Longman, I. M., 1963. A Green's function for determining the deformation of the Earth under surface mass loads. J. geophys. Res. 68, 485-496.

Love, A. E. H., 1909. The Yielding of the Earth to Disturbing Forces. Proc. Roy. Soc. London. 82, 73-88.

Luzum, B., and Coauthors, 2011. The IAU 2009 system of astronomical constants: The report of the IAU working group on numerical standards for Fundamental Astronomy. Celestial Mechanics and Dynamical Astronomy. 110(4), 293-304.

Melchior, Paul., 1974. Earth Tides. Surveys in Geophysics. 1, 275-303.

Monnereau, M., Calvet, M., Margerin, L., Souriau, A., 2010. Lopsided Growth of Earth's Inner Core. Science. 328(5981), 1014-1017.

Munk, W., 1997. Once again-Tidal friction. Progr. Oceanogr. 40, 7-35.

National Research Council (U.S.)., 1964. Panel on Solid Earth Problems. Solid-Earth Geophysics: Survey and Outlook. National Academies.

National Research Council (U.S.)., 1993. Solid-Earth sciences and society. National Academy Press, Washington.

Ozawa, H., Takahashi, F., Hirose, K., Ohishi, Y., Hirao, N., 2011. Phase Transition of FeO and Stratification in Earth's Outer Core. Science. 334(6057), 792-794.

Parke, M. E., and Hendershott, M. C., 1980. M_2, S_2, K_1 models of the global ocean tide on an elastic Earth. Mar. Geod. 3, 379-408.

Pekeris, C. L., and Accad, Y., 1969. Solution of Laplace's equations for the M2 tide in the world oceans. Philos. Trans. R. Soc. A. A265, 413-436.

Phillips, O. M., 1974. Nonlinear dispersive waves. Annual Review of Fluid Mechanics. 6, 93-110.

Pidwirny, M., 2006. Introduction to the Oceans (Fundamentals of Physical Geography, 2nd Edition).

Platzman, G. W., 1975. Normal Modes of the Atlantic and Indian Oceans. Journal of Physical Oceanography. 5(2), 201-221.

Platzman, G. W., 1978. Normal Modes of the World Ocean. Part I. Design of a Finite-Element Barotropic Model. Journal of Physical Oceanography. 8, 323-343.

Platzman, G. W., 1983. World Ocean Tides Synthesized from Normal Modes. Science. 220, 602-604.

Platzman, G. W., 1984. Normal Modes of the World Ocean. Part IV: Synthesis of Diurnal and Semidiurnal Tides. Journal of Physical Oceanography. 14, 1532-1550.

Proudman, J., and Doodson, A. T., 1924. The principal constituents of the tides of the North Sea. Philosophical Transactions of the Royal Society of London. A224, 185-219.

Proudman, J., 1953. Dynamical Oceanography. London: Methuen and Co., 409 pp.

Provost, C. L., Gence, M. L., Lyard, F., 1994. Spectroscopy of the world ocean tides from a finite element hydro dynamic model. J. Geophys. Res. 99, 24777-24797.

Pugh, D. T., 1987. Tides, Surges and Mean Sea-Level. JOHN WILEY & SONS.

Pugh, D. T., and Woodworth, P. L., 2014. Sea-Level Science: Understanding Tides, Surges Tsunamis and Mean Sea-Level Changes. Cambridge Univ. Press, Cambridge.

Ray, R. D., 1999. A global ocean tide model from Topex/Poseidon altimetry: GOT99.2. NASA Tech. Memo. 209478, 58 pp., Goddard Space Flight Center, Greenbelt, MD.

Redfield, A. C., 1980. The Tides of the Waters of New England and New York. Woods Hole: Woods Hole Oceanographic Institution, 108 pp.

Robert, H. S., 2008. Introduction To Physical Oceanography. Texas A& M University.

Roy, A. E., 1978. Orbital Motion. Adam Hilger, Bristol.

Sager, G., and Sammler, R., 1975. Atlas der Gezeitestrome fur die Nordsee, den Kanal und die Irische See. Deutschen Demokratischen Republic. Seehydrographischer Dienst, Nr. 8736. 3rd edn, ix, 58 pp.

Scherneck, H.-G., 1991. A parametrized solid Earth tide model and ocean tide loading effects for global geodetic baseline measurements. Geophys. J. Int. 106(3), 677-694.

Schettino, A., 2014. Quantitative Plate Tectonics. Springer International Publishing.

Schureman, P., 1976. Manual of Harmonic Analysis and Prediction of Tides. United States Government Printing Office, Washington.

Schwiderski, E. W., 1979. Global ocean tides: Part II. The semidiurnal principal lunar tide 84 (M_2), Atlas of Tidal Charts and Maps. NSWC Tech. Rep. 79-414.

Segar, D. A., 2012.Waves Introduction to Ocean Sciences (electric book), 2nd edition.

Shum, C. K., et al., 1997. Accuracy assessment of recent ocean tide models. J. Geophys. Res. 102, 25, 173-25, 194.

Shanmugam, G., 2014. Review of research in internal-wave and internal-tide deposits of China: Discussion. Journal of Palaeogeography. 3, 332-350.

Shepard, F. P., 1975. Progress of internal waves along submarine canyons. Marine Geology. 19, 131-138.

Simon, J. L., et al., 1994. Numerical expressions for precession formulae and mean elements for the Moon and planets. Astronomy and Astrophysics. 282 (2), 663-683.

Smart, W. M., 1940. Spherical Astronomy. Cambridge University Press.

Stammer, D., et al., 2014. Accuracy assessment of global barotropic ocean tide models. Rev. Geophys.. 52, 243-282.

Stevens, C. L., et al., 2012. Tidal Stream Energy Extraction in a Large Deep Strait: the Karori Rip, Cook Strait. Continental Shelf Research. 33, 100-109.

Stixrude, L., and Cohen, R. E., 1995. High-Pressure Elasticity of Iron and Anisotropy of Earth's Inner Core. Science. 267 (5206), 1972-1975.

Taylor, G. I., 1921. Tidal oscillations in gulfs and rectangular basins. Proceedings of the London Mathematical Society. 20, 148-81.

Thomson, W., 1879. On gravitational oscillations of rotating water. Proc. Roy. Soc. Edinburgh. 10,92-100.

Vlasenko, V., Stashchuk, N., Hutter, K., 2005. Baroclinic Tides: Theoretical Modeling and Observational Evidence. Cambridge Univ. Press, Cambridge.

Visser, P. N. A. M., et al., 2010. Space-borne gravimetric satellite constellation and ocean tides: Aliasing effects. Geophys. J. Int. 181, 789-805.

Voigt, C., et al., 2016. Report on the Data Base of the International Geodynamics and Earth Tide Service (IGETS), (Scientific Technical Report STR – Data; 16/08), Potsdam: GFZ German Research Centre for Geosciences.DOI:doi.org/10.2312/GFZ.b103-16087.

Wootton, A., 2006. Earth's Inner Fort Knox. Discover. 27 (9), 18.

Wieczorek, M. A., et al., 2006. The constitution and structure of the lunar interior. Reviews in Mineralogy and Geochemistry. 60(1), 221-364.

Williams, D. R., 2013. Sun Fact Sheet, NASA Goddard Space Flight Center.